FEATURE ARTICLE

Stereodynamics of Chlorine Atom Reactions with Organic Molecules

Craig Murray,† Julie K. Pearce, Svemir Rudić, Bertrand Retail, and Andrew J. Orr-Ewing*

School of Chemistry, University of Bristol, Cantock's Close, Bristol BS8 1TS, U.K.

Received: August 17, 2005; In Final Form: October 4, 2005

A series of recent experimental and computational studies has explored how the dynamics of hydrogen abstraction from organic molecules are affected by the presence of functional groups in the molecule and by basic structural motifs such as strained ring systems. Comparisons drawn between reactions of Cl atoms with alkanes such as ethane, $Cl + CH_3CH_3 \rightarrow HCl + CH_3CH_2$, which serve as benchmark systems, and with functionalized molecules such as alcohols, amines, and alkyl halides, $Cl + CH_3X \rightarrow HCl + CH_2X$ (X = OH, NH_2, halogen, etc.) expose a wealth of mechanistic detail. Although the scattering dynamics, as revealed from measured angular distributions of the velocities of the HCl with quantum-state resolution, show many similarities, much-enhanced rotational excitation of the HCl products is observed from reactions of the functionalized molecules. The degree of rotational excitation of the HCl correlates with the dipole moment of the CH_2X radical and is thus attributed, at least in part, to post-transition-state dipole−dipole interactions between the separating, polar reaction products. This interpretation is supported by direct dynamics trajectories computed on-the-fly, and the HCl rotation is thus argued to serve as an in situ probe of the angular anisotropy of the reaction potential energy surface in the post-transition-state region. Comparisons between the dynamics of reactions of dimethyl ether and the three- and four-membered-ring compounds oxirane (c-C_2H_4O) and oxetane (c-C_3H_6O) raise questions about the role of reorientation of the reaction products on a time scale commensurate with their separation. The shapes and structures of polyatomic molecules are thus demonstrated to have important consequences for the stereodynamics of these direct abstraction reactions.

1. Introduction

The field of stereodynamics explores what has been dubbed the *chemical shape* of a molecule.[1,2] This concept embodies how the geometries of approach of two reacting species affect their reactivity (e.g., what is the most favorable orientation for reaction?), or how molecular shapes and structures influence the dynamics of a reactive collision during approach to, and separation from, a transition state (TS). The chemical shape will generally differ from the physical shape, as determined by spectroscopy and parametrized by a collection of bond lengths and angles. A global potential energy surface (PES) will reveal chemical shape through, for example, examination of how the forward or reverse barrier to a TS, and thus the reaction probability, depends on the angle of attack or the relative orientations of the reagents. Quantum mechanical (QM) or classical scattering calculations on such global PESs then address how the dynamics of motion of all the participant atoms are influenced by the chemical shape. Chemically accurate PESs are only available for few reactions, however, and most of these involve just three atoms (denoted nonspecifically as A, B, and C) and are of the type:

$$A + BC \rightarrow AB + C \qquad (1)$$

A combination of experimental and theoretical studies of such atom-transfer reactions has proved immensely profitable,[3] as illustrated by the wealth of knowledge obtained about fundamental dynamics (i.e., how the relative positions and velocities of the atoms change with time during the reaction), as well as more exotic features of chemical reactivity such as scattering resonances,[4,5] nonadiabatic dynamics on multiple PESs,[6,7] or geometric phase effects.[8] The well-established benchmark systems for direct reactions are the hydrogen exchange reaction ($H + H_2 \rightarrow H_2 + H$ and isotopic variants such as $D + H_2 \rightarrow HD + H$),[9] and the reaction of fluorine atoms with H_2 ($F + H_2 \rightarrow HF + H$)[10] because quantitative comparisons can be made between state-of-the-art experimental measurements and theoretical treatments. Theoretical methods can incorporate fully ab initio PESs computed from electronic structure theory, QM scattering calculations, and allowance for breakdown of the Born−Oppenheimer approximation (nonadiabatic dynamics). The stereodynamics of these "elementary" reactions are now best understood from analysis of the outcomes of scattering calculations on the best available PESs, using both QM and classical trajectory methods, as illustrated by the recently demonstrated "stereodynamical portraits" of the hydrogen exchange reaction.[11]

There are nevertheless clear limitations to studies restricted to reactions involving just three atoms, most important of which, for the context of the current article, will be that the consequences of shape and structure of the species C cannot be explored. Moving up to a four-atom (or larger) reaction:

$$A + BCD \rightarrow AB + CD \qquad (2)$$

additional features of the dynamics merit serious attention: *both*

* Author for correspondence. Tel: +44 117 928 7672. Fax: +44 117 925 0612. E-mail: a.orr-ewing@bris.ac.uk.

† Current address: Department of Chemistry, University of Pennsylvania, 231 South 34th Street, Philadelphia, PA 19104.

10.1021/jp054627l CCC: $30.25
Published on Web 11/04/2005

Craig Murray received his B.Sc. degree in Chemistry from The University of Edinburgh in 1997 and remained there to complete a Ph.D. under the direction of Kenneth G. McKendrick. From 2001 to 2004 he was employed as a postdoctoral research assistant at the University of Bristol. He currently works with Marsha I. Lester at the University of Pennsylvania, where he holds the position of Dreyfus Fellow in Environmental Chemistry. His current research involves the production and characterization of weakly bound complexes relevant to atmospheric chemistry and studies of collision-induced electronic quenching.

Julie Pearce studied Chemistry at the University of York and graduated with an M.Chem. degree in 2003. She then moved to the University of Bristol where she is currently studying for her Ph.D. Her research interests focus on the dynamics of chlorine atom reactions with organic molecules.

Svemir Rudić received a B.Sc. in Physics from the University of Zagreb in 1998 and a Ph.D. in Physical Chemistry in 2003 from the University of Bristol. After postdoctoral work at the University of North Carolina, Chapel Hill, he returned to the University of Bristol for further postdoctoral studies. His current research focuses on characterizing the optical properties of aerosol particles.

Bertrand Retail received his B.Sc. and M.Sc. degrees in Chemical Physics from the University of Bordeaux I. He began graduate studies at the University of Bristol in 2004. His current research concerns the application of velocity-map ion imaging to crossed molecular beam techniques to study the dynamics of bimolecular reactive scattering, with particular focus on the effect of nonadiabatic interactions in chemistry.

Andrew J. Orr-Ewing obtained his B.A. and M.A. degrees in Chemistry and his doctorate in Physical Chemistry from the University of Oxford. After a two-year period as a postdoctoral researcher at Stanford University, he joined the University of Bristol, first as the Eliz. Challenor Research Fellow of the Royal Society, and subsequently as a lecturer. He currently holds a chair in Physical Chemistry. His group has research interests in chemical reaction and photodissociation dynamics and applications of laser based techniques to the study of atmospheric chemistry and the chemistry of plasmas and thin-film deposition.

the AB and CD products can carry off internal energy as vibrational and rotational motion (the latter having consequences for angular momentum conservation), there may well be correlations between the extent of vibrational and rotational excitation of the two products (which can now be mapped experimentally), and the products can potentially interact via permanent dipolar and higher order anisotropic long-range electrostatic forces as they separate.

A number of benchmark systems are becoming established for reactions between atoms and triatomic or larger molecules, most notable of which are $H + H_2O \rightarrow H_2 + OH$[12,13] and $X + CH_4 \rightarrow HX + CH_3$ (with X = H, F and Cl),[14−17] for which useful comparisons between experiment and theory are now available. The reactions of Cl atoms with other, higher alkanes, have also received considerable experimental attention[17] and will serve as important sources of comparison for the Cl atom reactions with functionalized organic molecules described here[18−25] and represented in a simplified form as

$$Cl + CH_3Y \rightarrow HCl + CH_2Y \quad (Y = OH, \text{halogen}, NH_2, -OCH_3, \text{etc.}) \quad (3)$$

It is implicit in this reaction scheme, and hereafter, that the Cl atom is in its ground electronic state ($^2P_{3/2}$) and not in the low-lying, spin−orbit excited-state Cl*($^2P_{1/2}$) with an additional 882 cm^{-1} of electronic energy. The various Cl atom reactions are attractive for a number of reasons beyond simple practical considerations of the feasibility of experimental investigation described in the following section. The main motivations for their study are as follows:

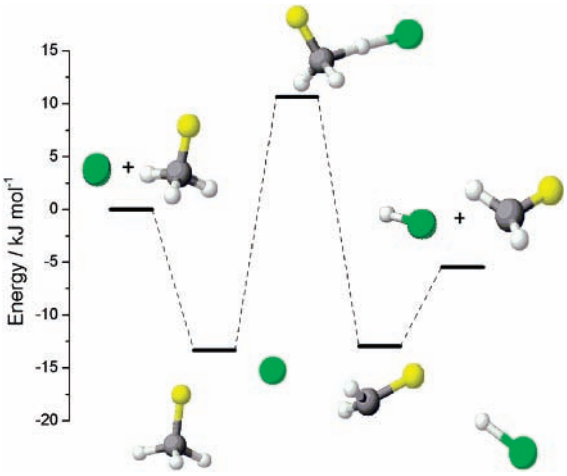

Figure 1. Potential energies of structures corresponding to minima and maxima along the pathway for the reaction $Cl + CH_3F \rightarrow HCl + CH_2F$. All energies were calculated at the G2//MP2/6-311G(d,p) level of theory, and the diagram illustrates the weakly bound pre- and post-transition-state complexes discussed in the text. Note also the near-collinear Cl−H−F configuration in the transition state.

(i) Pathways for the various reactions in eq 3 exhibit energetically low-lying transition states, with shallow wells in the entrance and exit valleys of the PES, corresponding to weakly bound pre- and post-transition-state complexes that may also influence the reaction dynamics. These features on the PES are illustrated in Figure 1 for the reaction of Cl atoms with CH_3F. The weakly bound complexes, and analogous ones for reactions of other atoms and radicals, are now amenable to direct spectroscopic investigation and thus structure determination within the very cold environments of pulsed molecular beams,[26] or helium nanodroplets.[27]

(ii) The thermodynamics of the reactions range from near-thermoneutral (in some cases slightly endothermic) to mildly exothermic, in stark contrast to the equivalent reactions of fluorine atoms, which are more strongly exothermic because of the formation of HF products. As a result, energy release to the fragments is small and the dynamics are unlikely to be dominated by impulsive release of excess energy from the transition state. Such impulsive dynamics can be interpreted using kinematic models,[28,29] but may mask more subtle dynamical effects of the type sought here that arise from the topology of the PES. The thermodynamics of some representative Cl atom reactions are listed in Table 1.[17,25,30]

(iii) The combination of low-energy release from the reactions and the mass of the Cl atom means that the speeds of recoil of the reaction products are sufficiently slow to allow reorientation dynamics of both the HCl and the organic radical coproduct (CH_2Y in eq 3) to occur while they are still within close proximity. The dynamics can thus sample geometries corresponding to interesting features on the PES, and the role of different reorientation behavior, influenced by the structure of the radical, can be explored. The geometry of the transition state at a saddle point on the PES is thus not the sole determinant of the preceding and subsequent dynamics.

(iv) As will be argued in section 3, the extent of rotational excitation of the HCl serves as an in situ probe of the effects outlined in (ii) and (iii) above. HCl has a sufficiently large rotational constant and thus dispersed spectrum for individual,

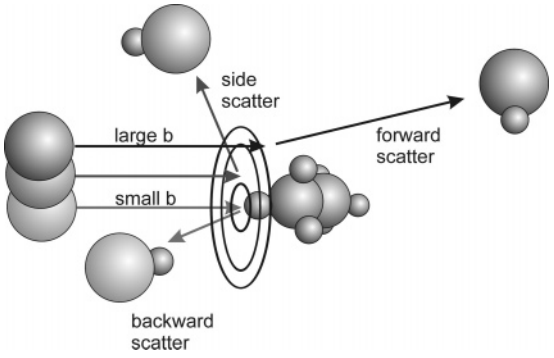

Figure 2. Schematic diagram of the effects of impact parameter (b, represented by the target rings around a C−H bond) on the HCl scattering direction for reaction of Cl atoms with ethane. Low-impact parameters (head-on collisions) lead to rebound dynamics and backward scatter, whereas larger impact parameter collisions result in reaction near the periphery of the molecule and a switch to sideways or forward scatter relative to the direction of approach of the Cl atom.

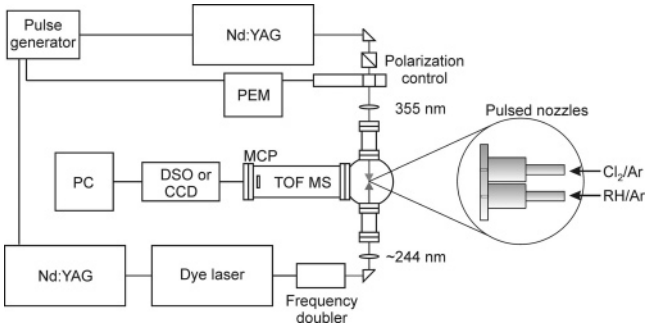

Figure 3. Schematic diagram of the laser and vacuum apparatus used to study photoinitiated reaction dynamics. The abbreviations used are as follows: PEM, photoelastic modulator; DSO, digital storage oscilloscope; CCD, charge coupled device camera; MCP, microchannel plate (coupled with a phosphor screen for imaging experiments); TOF MS, time-of-flight mass spectrometer. Twin pulsed nozzles inject reagent gases into a high-vacuum chamber prior to the photolysis and probe laser pulses; the gas flows are, in some instances, merged using PTFE tubes.

rotationally resolved transitions to be probed using standard pulsed laser systems.

(v) The products of reaction 3 are generally broadly scattered in all directions relative to the approach velocity of the Cl and CH_3Y (i.e., the relative velocity vector), giving center-of-mass frame scattering in forward, sideways, and backward directions. As with the reactions of Cl atoms with alkanes other than methane, such broad scattering is attributed to the effects of reaction at a range of impact parameters from head-on type collisions (favoring backward scatter) to skimming the periphery of the molecule (large impact parameters) that favors stripping dynamics and forward scattering.[17] This behavior is illustrated schematically in Figure 2 for reaction of Cl atoms with ethane. There are few, if any steric restrictions on the reactivity because of low or nonexistent activation barriers and a weak dependence of the barrier height on attack angle.

(vi) Various structural motifs present in simple organic molecules (e.g., polarity, straight chain versus cyclic skeletons) can be used to explore dynamical effects. The consequences of structure on the stereodynamics will be examined in detail in section 3.

This article is organized in the following way: in section 2, experimental strategies used to explore the stereodynamics of Cl atom reactions with organic molecules are summarized; results of such measurements, along with complementary dynamical calculations are described in section 3; an overview of the conclusions drawn from the large data set, and future prospects are presented in section 4.

2. Experimental Strategies

Much of the existing literature on the stereodynamics of chemical reactions describes the use of either pre-*oriented* or pre-*aligned* reagents (a subtle distinction depending on whether the collisions distinguish one end from the other, or side-on from end-on attack),[1,2,28] or the measurement of angular momentum alignment of the products, which depends on the way the products rotate in space, and thus the directions of torques applied over the course of the reaction.[31] There are several journal special issues and review articles that address such measurements,[31−34] and they will not be discussed further here. In the current investigations, the experimental strategy employed is instead to generate Cl atoms photolytically from Cl_2, in proximity to a co-reagent organic molecule, and detect the HCl products with rotational- and vibrational-quantum-state specificity. Measurements can determine the relative populations of different rotational levels of the HCl, thus distinguishing low and high rotational excitation, as well as the directions of scatter of the products. The distribution of scattering angles, suitably renormalized, is referred to as the differential cross section and describes the correlation between the relative velocity vectors of the reagents and products.

Figure 3 shows a schematic diagram of the types of apparatus used for the experimental measurements. Cl_2 photolysis is conveniently carried out at 355 nm using the third harmonic of an Nd:YAG laser and produces almost exclusively ground spin−orbit-state Cl atoms that are near-monoenergetic with a speed of 1660 m/s. HCl detection is best achieved by 2+1 resonance enhanced multiphoton ionization (REMPI), via absorption of two ultraviolet photons from a tuneable, pulsed laser to reach either the F $^1\Delta$ or f $^3\Delta$ Rydberg state, both of which exhibit well-resolved rotational fine structure, followed by absorption of one further photon to ionize the highly excited HCl. The resultant HCl^+ molecular ions are collected and measured using

TABLE 1: Thermochemistry of Cl-Atom Reactions with Selected Organic Molecules[17,25,30]

reaction	ΔH_{298}/kJ mol^{-1}	comments
$Cl + C_2H_6 \rightarrow HCl + C_2H_5$	-8.7 ± 1.6	
$Cl + C_3H_8 \rightarrow HCl + n\text{-}C_3H_7$	-8.3 ± 2.1	primary H abstraction
$Cl + C_3H_8 \rightarrow HCl + i\text{-}C_3H_7$	-22.5 ± 2.0	secondary H abstraction
$Cl + CH_3OH \rightarrow HCl + CH_2OH$	-29.8 ± 1.3	
$Cl + CH_3F \rightarrow HCl + CH_2F$	-12.8 ± 8.4	
$Cl + CH_3Cl \rightarrow HCl + CH_2Cl$	-14.4 ± 3.2	
$Cl + CH_3Br \rightarrow HCl + CH_2Br$	-6.5 ± 4.4	
$Cl + CH_3I \rightarrow HCl + CH_2I$	$+2.3 \pm 6.8$	
$Cl + CH_3NH_2 \rightarrow HCl + CH_2NH_2$	-41.8 ± 1.9	
$Cl + CH_3NH_2 \rightarrow HCl + CH_3NH$	-13.8 ± 1.9	
$Cl + c\text{-}C_2H_4O \rightarrow HCl + c\text{-}C_2H_3O$	-8.4 ± 12.5	ring opening to form vinoxy radicals is -148.1 ± 3.8 kJ mol^{-1} exothermic

a time-of-flight mass spectrometer to distinguish them from ions formed by other processes such as UV laser ionization and fragmentation of the organic reagent. The intensities of the REMPI lines are affected by two-photon line strengths and processes that compete with ionization such as predissociation of the states accessed at the 2-photon level, but calibration to convert measured line intensities to relative populations is straightforwardly achieved using spectra of a dilute, room-temperature sample of HCl.[19] The products must be detected under conditions in which they have not undergone secondary collisions with surrounding gas molecules (which might otherwise alter their rotational energies), and before they fly out of the probe laser volume. Hence, experiments are conducted at very low pressures ($<10^{-4}$ Torr), and at short (<100 ns) time delays between the photolysis and probe laser pulses. As a result, experimental signals can be very low and thus very sensitive detection techniques, such as 2+1 REMPI, must be used to monitor the reaction products. It is imperative to eliminate any contaminant HCl in the source gases because this will give REMPI signals that overwhelm the weak reactive signal. Very high-purity Cl_2 is thus used, and premixing of the Cl_2 and organic reagent is avoided by keeping them separate until they are injected into the high-vacuum chamber, at which point they mix just before the time the laser pulses are fired. The probe laser is fired at twice the repetition rate of the photolysis laser, allowing shot-by-shot subtraction of background HCl signals. Despite such precautions, contaminant HCl rapidly builds up, probably through reaction of Cl_2 and water on the stainless steel walls of the pulsed nozzle and gas delivery line. The effects can, however, be temporarily alleviated by introducing small amounts of NO to the gas handling line when the HCl contamination exceeds manageable levels.

Two methods of detection of the HCl^+ ions have proved fruitful for the dynamical studies. The first is to collect the integrated ion signal at a time-of-flight after the ionizing laser pulse that corresponds to a mass-to-charge ratio of 36.[18−20,23,25] As the probe laser wavelength is scanned across the region of HCl absorption to the F $^1\Delta$ and f $^3\Delta$ states, the resultant signals give a spectrum for the nascent reaction products, and assignment of the spectroscopic lines, combined with the correction factors described above, allows relative populations of different rotational levels of HCl X $^1\Sigma^+$ ($v' = 0$) to be derived. These levels are labeled by a rotational quantum number J'. From the populations, rotational temperatures are extracted using a Boltzmann analysis. Alternatively, the recoil velocities of the HCl products can be obtained using the velocity map imaging technique and a position-sensitive detector (in this case a microchannel plate and phosphor screen combination, with points of impact recorded as bright spots on the screen using a CCD camera connected to a computer).[22,24] The experimental setup used for velocity map imaging experiments has been described in detail previously and makes use of a pair of pulsed nozzles, aligned parallel to one another, together with photolytic production of Cl atoms. As described in refs 22 and 24, this arrangement allows the scattering distribution in the center-of-mass frame to be obtained directly from the resultant images.

3. Outcomes and Theoretical Approaches

In this section, the results are presented of representative measurements of the stereodynamics of Cl atom reactions. With a wealth of accumulated data,[17−25] correlations and trends can be sought, and some general comments made about classes of reactions. This is an important outcome if understanding is to be sought of patterns of dynamical behaviour, rather than focusing on every reaction as individual and unique. The reaction systems are prohibitively large for sufficiently accurate calculations of global PESs, or for QM scattering calculations, and thus without the full weight of modern quantum chemical methods to fall back on for interpretation of experimental results, deductions presented here remain somewhat speculative. Nevertheless, the arguments presented are supported by evidence from the best available theory: in the case of the many-atom reactions being studied, this corresponds to the classical trajectory calculations carried out by the Bristol group, with on-the-fly calculation of potential energies and forces that control the trajectories using electronic structure theory packages.[21] In on-the-fly methods, the electronic structure calculations are performed only at geometries sampled by a trajectory, and the results are used to propagate the trajectory on to its next geometry. Such calculations enable animations to be constructed of the atomic motions over the course of a reactive trajectory, and batches of hundreds or thousands of trajectories can be run to compute distributions of internal and translational energies of the products for comparison with experimental data. There are several weaknesses of these trajectory calculations, and these are highlighted up-front here so the reader is aware of their limitations. Nevertheless, they remain the best available theoretical resource for interpretation of experimental outcomes because quasi-classical trajectory (let alone quantum mechanical scattering) calculations on a fully dimensional global PES are beyond the scope of current computer resources and theoretical methodologies. The GROW interpolation strategy of Collins and co-workers[35,36] presents an exciting possibility to improve radically on this situation, as do developments by Kerkeni and Clary[37] in reduced dimensionality quantum dynamics.

The methods used for the on-the-fly classical trajectory calculations are described in detail in ref 21, and only a brief summary is given here. Trajectories are launched from the transition state of the reaction (for reasons of computational expediency), with initial conditions of positions and momenta of nuclei undergoing vibrational motion selected randomly from a Wigner distribution for all zero-point modes of the transition-state structure. The calculations thus neglect the approach of reagents to the transition state (with a range of impact parameters and orbital angular momenta), the effects of shallow wells in the entrance valleys of the PES, and the possibility of excitation above the zero-point level of, in particular, low-frequency transition-state modes. The trajectories are started by providing energy along the reaction coordinate in the direction of products and are propagated using a velocity Verlet algorithm. At each time step along the trajectory, electronic structure theory calculations evaluate the potential energy and the gradients of the PE function, and the associated forces (and thus accelerations) are applied to propagate the atoms to the positions corresponding to the next time step. This process is repeated as many times as necessary for the trajectories to evolve to reach some criteria (e.g., center-of-mass separation, converged and stable angular momentum) used to judge that products have successfully formed. This process may require as many as 1000−2000 time steps per trajectory and is thus very time-consuming if the levels of ab initio quantum theory or density functional theory (DFT) used to compute the PE functions are sufficient for a realistic representation of the reaction. A sufficiently accurate functional for DFT calculations of the energetics of the Cl atom reactions has yet to be found, and calculations presented here are thus restricted to the use of either Hartree−Fock theory with a 6-31G basis set (for which one trajectory takes ∼30 min on a node of a pc cluster) or MP2

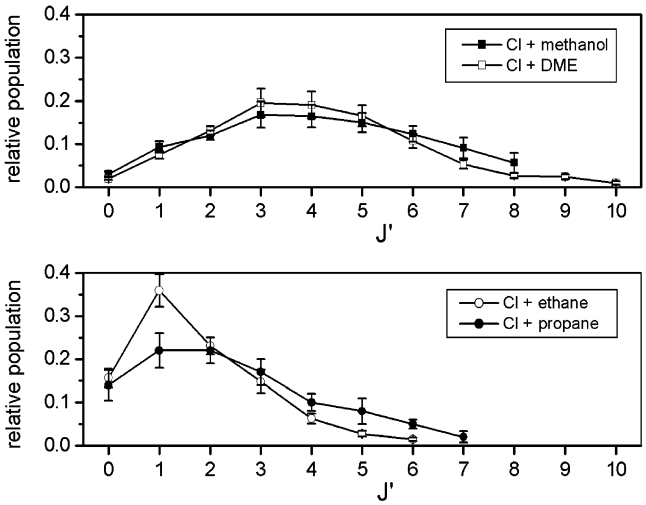

Figure 4. Distributions of relative populations of the rotational levels of the HCl($v' = 0$) products of various reactions. J' denotes the HCl rotational quantum number. Bottom panel: reaction of Cl atoms with representative alkanes, (○) ethane and (●) propane (data from ref 38). Top panel: reactions of Cl atoms with (■) methanol and (□) dimethyl ether. All distributions are normalized so that they sum to unity.

calculations with a 6-311G(d,p) basis set (up to 3 days per trajectory). Batches of 200−2000 trajectories thus require very large amounts of dedicated computer time, and a balance has to be struck between computational accuracy and the available computer resources. The level of ab initio theory must thus also be regarded as a limitation of the calculations, although methods are used that give a reasonable approximation of the energy differences between the transition state and the products, as computed at the G2//MP2/6-311G(d,p) level of theory, which has been shown to be reliable for the various reactions studied.

A further important limitation is the use of classical mechanics for the trajectories. Although the nuclear dynamics are likely to be well represented by this approach, with QM effects such as tunneling, quantum bottleneck states, or reactive scattering resonances playing no clear role in influencing the experimental data, correct treatment of the large zero point energy of the whole system is not possible with the classical trajectories.

3.1. HCl Rotational Distributions. Previous studies of the kinetics of reactions of Cl atoms with a variety of organic molecules already provide some mechanistic insights, although there are many gaps in the reactions investigated. Much of the existing body of literature has been summarized in a recent review article[17] and will not be revisited in depth here. Representative hydrogen abstraction reactions from molecules such as alkanes (other than methane) and alcohols have no, or only very low, barriers to reaction, and hence large rate coefficients ($k > 10^{-11}$ molecule^{-1} cm^3 s^{-1} at 298 K). The reactions with methyl halides have low activation barriers and rate coefficients at 298 K in the range 10^{-13} to 10^{-12} molecule^{-1} cm^3 s^{-1}. H-atom abstraction is generally most favorable from the carbon atom bonded directly to the heteroatom (the α-C atom) and, with the exception of the methyl halides, is more exothermic than abstraction of a primary H-atom from an alkane. Barriers to abstraction of H atoms from the OH group of an alcohol are significantly higher than for reaction at a C−H bond, and formation of alkoxy radicals has been shown to be a negligible pathway, even at the higher collision energies used in reaction dynamics experiments.[18,19] Kinetic studies of the reactions of Cl atoms with amines are sparse, but reaction of methylamine can lead to both the methanaminyl (CH_3NH) and the aminomethyl (CH_2NH_2) radicals.[20]

TABLE 2: Summary of the Mean Rotational Energies and Rotational Temperatures of the Nascent HCl($v' = 0$) Products of Various Reactions Discussed in the Text

reaction	$\langle E_{rot}\rangle$/cm^{-1}	T_{rot}/K
$Cl + CH_4 \rightarrow HCl + CH_3$	64 ± 4	88 ± 6
$Cl + C_2H_6 \rightarrow HCl + C_2H_5$	69 ± 5	117 ± 5
$Cl + C_3H_8 \rightarrow HCl + C_3H_7$	117	
$Cl + CH_3OH \rightarrow HCl + CH_2OH$	330 ± 29	530 ± 56
$Cl + CH_3OCH_3 \rightarrow HCl + CH_2OCH_3$	265 ± 17	418 ± 25
$Cl + CH_3F \rightarrow HCl + CH_2F$	284 ± 13	403 ± 18
$Cl + CH_3Cl \rightarrow HCl + CH_2Cl$	283 ± 21	380 ± 20
$Cl + CH_3Br \rightarrow HCl + CH_2Br$	226 ± 14	302 ± 12
$Cl + CH_3I \rightarrow HCl + CH_2I$	202 ± 13	291 ± 26
$Cl + CH_3NH_2 \rightarrow HCl + CH_2NH_2$	501 ± 84	720 ± 210
$Cl + CH_3NH_2 \rightarrow HCl + CH_3NH$	122 ± 12	181 ± 16
$Cl + c\text{-}C_2H_4O \rightarrow HCl + c\text{-}C_2H_3O$	98 ± 7	168 ± 7
$Cl + c\text{-}C_3H_6O \rightarrow HCl + c\text{-}C_3H_5O$	272 ± 11	399 ± 23

Figure 4 shows representative HCl rotational level population distributions for reactions of Cl atoms with ethane and propane (results for methane and *n*-butane are very similar), and with methanol and dimethyl ether (DME).[17,19,38] In Table 2, a larger collection of such data is summarized in the form of HCl rotational temperatures and mean rotational energies. Although the nascent rotational distributions need not, a priori, be well described by a Boltzmann distribution corresponding to a single temperature, such a parametrization turns out to work satisfactorily. The first striking observation is that, in the case of most of the reactions of functionalized molecules, the HCl is formed with considerably greater rotational excitation than from the reactions with alkanes: the energy releases for the former reactions are, in some cases, larger, but there is no clear correlation between HCl rotational excitation and the enthalpy of reaction. The established wisdom for the Cl + alkane reactions is that the transition state is preferentially collinear in the Cl−H−C moiety, and this, combined with nonimpulsive release of the energy of the reaction, applies little or no torque to the departing HCl, which is thus formed rotationally very cold.[17]

Why, then, are the HCl molecules rotationally so much hotter from the reaction of Cl atoms with methanol, ethanol, and several other functionalized organic molecules? Exothermicity may play a part, but as mentioned above, there is not a clear-cut correlation, and exceptions stand out such as the reactions of Cl with the methyl halides. If the dynamics are impulsive, bent transition states will tend to produce rotationally excited products,[39] particularly if, as in the current reactions, a light atom (H) is transferred. The computed transition-state equilibrium structures for all the reactions considered here in which an H atom is abstracted by chlorine from a carbon atom, however, deviate only very slightly (by just a few degrees) from a collinear C−H−Cl arrangement, much as is observed for reactions of Cl atoms with alkanes. Low transition-state bending frequencies of the C−H−Cl group might project on to HCl rotational motion, but the bending potentials for ethane and higher alkane reactions with chlorine atoms also show low bending frequencies. For example, for reaction of Cl with methanol, the computed bending frequencies at the TS (at the MP2/6-311G(d,p) level of theory) corresponding to motion of the transferring H-atom, are 66 and 165 cm^{-1}, and for the ethane reaction they are 117 and 172 cm^{-1}. By way of contrast, the Cl−H−CH_2Cl transition state, which sits atop a low barrier, is tighter (at least in one coordinate), with computed bending frequencies of 108 and 349 cm^{-1}, yet still results in rotationally hot HCl. The evidence from the trajectory calculations suggests that although the mean HCl rotational energies are not controlled

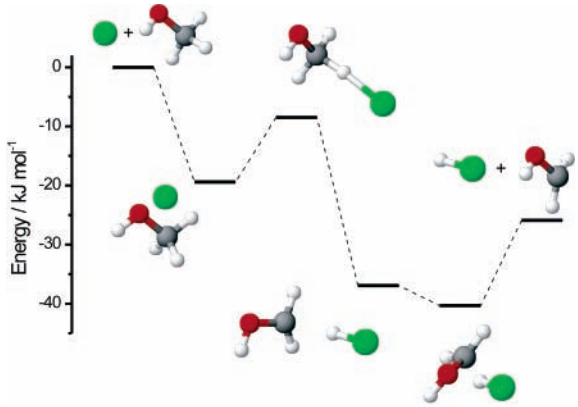

Figure 5. Computed energies and structures corresponding to stationary points on the PES for reaction of Cl atoms with methanol. The calculations were performed at the G2//MP2/6-311G(d,p) level of ab initio electronic structure theory.

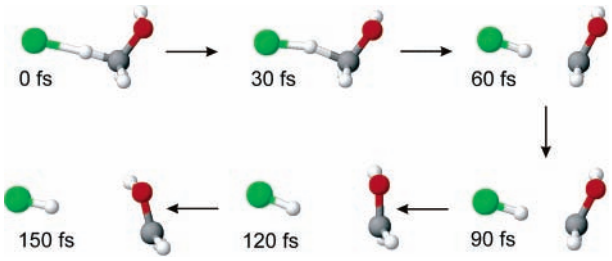

Figure 6. Snapshots and time intervals taken from a classical trajectory with on-the-fly ab initio calculation of potential energies and gradients, illustrating the first 150 fs of evolution of molecular geometries from the transition state of reaction of Cl atoms with methanol. The figure shows the start of reorientation of the O-atom end of the hydroxymethyl radical toward the HCl molecule; their subsequent interaction maps, at later time, onto enhanced HCl rotational motion.

by TS bending vibrations, these motions do strongly influence the *widths* of the rotational distributions.

Examination of the stationary points along the minimum energy pathway for reaction, as illustrated for Cl + CH_3F in Figure 1 and Cl + CH_3OH in Figure 5, suggests an alternative explanation. Rudić et al.[18−20] and Murray et al.[23] proposed that the source of the HCl rotational excitation was post-TS interactions between the two polar species, the organic radical and the HCl, prior to their separation beyond the range of dipolar and higher order electrostatic forces. The angular anisotropy of these forces, combined with favorable reorientation dynamics of the two products toward a hydrogen-bonded minimum energy structure on the PES, can induce HCl rotation. The reorientation is caused by the torque induced about the center of mass of the radical as the H-atom is transferred and naturally pushes the polar functional group toward the slowly departing HCl. An acceleration of the HCl rotational motion is clearly evident in trajectories as the rotation of the radical brings the (generally) negative end of its dipole into proximity with the positively polarized H-atom end of the diatomic molecule. The initial post-TS dynamics are illustrated schematically in Figure 6, which takes a sequence of frames from an animation of the early stages of an on-the-fly trajectory for the reaction of Cl atoms with methanol initiated at the TS; the intermediate structures evolve toward the weakly bound post-TS complex for this reaction evident in the PE profile of Figure 5. Apart from the on-the-fly trajectory outcomes, there is further evidence to support the asserted mechanism. A simple calculation of the energy gained by reorientation of the incipient dipoles on the CH_2OH and HCl from their near-perpendicular geometry in the TS to the near-parallel geometry arising in the post-TS complex, corresponds very closely with the experimentally measured mean rotational energy of the HCl products. Even more compelling is the strong linear correlation (plotted in Figure 10 of ref 17) observed between the mean HCl rotational energy and the dipole moment of the organic radical (as computed at the MP2/6-311G(d,p) level of theory) for reactions of Cl atoms with CH_3OH, CH_3CH_2OH, CH_3OCH_3, CH_3F, CH_3Cl, CH_3Br, CH_3CH_3, and CH_4. Exceptions to this correlation, and possible reasons, are discussed in more detail below.

It is worth noting in passing that calculations using a statistical prior model,[28] that treat the radical coproduct either as structureless or a linear rigid rotor, considerably overestimate the extent of HCl rotational excitation for the reaction of Cl atoms with CH_3OH. Statistical partitioning of rotational energy into the various degrees of freedom of the products is thus discounted, and an interpretation in terms of a direct dynamical mechanism is preferred. For three-atom reactions involving transfer of a light atom (L) between two heavier atoms (H), denoted as H + LH → HL + H, kinematic constraints imposed by conservation of angular momentum result in efficient mapping of reagent to product orbital angular momentum. There are consequent effects for the amount of rotational angular momentum of the newly formed diatomic molecule. Such constraints on the HCl rotational motion will be relaxed, however, for the reactions considered here because the polyatomic radical coproduct can also carry considerable amounts of rotational angular momentum at little cost in energy.

Analysis of the outcomes of batches of hundreds of trajectory calculations generates rotational level population distributions that can be compared to experimental measurements. The shape of the calculated distribution for reaction of Cl + CH_3OH is in excellent agreement with that plotted in Figure 4, but the calculations overestimate the J' value at the peak of the distribution by 1 or 2 units of angular momentum, with the smaller discrepancy for MP2/6-311G(d,p) level calculation of potential energy terms. This overestimation of rotational excitation is consistent with the corresponding computed dipole moments, which are also calculated to be larger than experimental values. The trajectory calculations have also been used to compute correlations between the rotational angular momentum ($\mathbf{J}'$) and relative velocity ($\mathbf{v}'$) vectors of the HCl and radical reaction products.[21] For reactions of Cl atoms with CH_4, C_2H_6, and CH_3OH, the distributions of angles between $\mathbf{v}'_{HCl}$ and $\mathbf{J}'_{HCl}$ are broad and peak at 90°, in reasonable agreement with the limited available experimental data.[40] The angles between $\mathbf{v}'_R$ and $\mathbf{J}'_R$ are similarly distributed for R = CH_3 and are likely to reflect a mapping of the initial TS angular momentum, whereas for R = C_2H_5 and CH_2OH, the radical velocity and rotational angular momentum vectors are much more sharply correlated mutually perpendicular. This latter result is a consequence of the torque applied by the departing H atom about the radical center of mass (which is now displaced from the line of force, unlike for CH_3); this torque generates a rotational angular momentum that dominates effects associated with any zero-point motion of the TS.

3.2. Effects of Dipole Orientation. The effects of post-TS interactions described so far are essentially scalar in nature, which is to say that the *magnitudes* of the dipole moments of the radical and HCl products have a determining effect on the rotational energy of the HCl. The vectorial properties of the dipole moments must, however, also be considered, and are well illustrated by the reaction of Cl with methylamine which can occur via two competing pathways (abstraction of an H atom from the C or the N atom) with near equal probabilities:[20]

$$Cl + CH_3NH_2 \rightarrow HCl + CH_2NH_2 \quad (4a)$$

$$Cl + CH_3NH_2 \rightarrow HCl + CH_3NH \quad (4b)$$

The pathways can be distinguished by use of the deuterated compounds CH_3ND_2 and CD_3NH_2, and by selective detection of DCl or HCl reaction products. The geometries of the transition states and pre- and post-TS complexes computed for these two reactions are shown in Figure 7. In Figure 8, the dipole moments are shown superimposed on structures of the post-TS complexes, as calculated at the MP2/6-311G(d,p) level of theory. As the products of reaction 4a separate, the positive end of the dipole moment of the CH_2NH_2, which resides at the NH_2 end, swings toward the positive end of the HCl dipole moment, initiating a repulsive interaction that induces counter-rotational motion of the HCl. For reaction 4b, in contrast, the dipoles of the CH_3NH and the HCl happen to be oriented parallel and nearly collinear, so any rotation of the HCl is opposed by a restoring force toward this lowest energy geometry. The electronic structure theory and trajectory calculations thus predict greater rotational excitation for the products of channel (4a) than for channel (4b) despite the computed TS for reaction 4b having a Cl−H−N bend angle of 142°, compared to a much more collinear Cl−H−C angle of 171° for channel (4a). Impulsive model calculations based on these transition-state structures predict precisely the opposite trend for HCl rotational excitation but are proved to be incorrect by the experimental measurements: the HCl formed in coincidence with CH_2NH_2 has a mean rotational temperature of 720 ± 210 K, whereas the HCl formed with CH_3NH is much more rotationally cold, with T_{rot} = 181 ± 16 K. The orientation of the charge separation in the two reaction products thus has a measurable influence on the reaction stereodynamics.

3.3. Reactions of Constrained Ring Compounds. The dynamics of three- and four-membered ring compounds can be compared directly with those for straight chain compounds to explore how such structural motifs influence the reaction mechanism. The four reactions of Cl atoms with methanol, dimethyl ether, oxirane (c-C_2H_4O), and oxetane (c-C_3H_6O) raise some interesting questions about the role of reorientational motion on the reaction dynamics. Rotational distributions for the HCl products of reactions of Cl atoms with the latter three of these four oxygen-containing molecules are plotted in Figure 9, and the results for the oxirane reaction clearly stand out as much more rotationally cold. A very similar result is obtained for reaction of Cl atoms with thiirane (C_2H_4S).[25] The existing evidence for the oxirane reaction supports a pathway that retains the three-membered ring, rather than the much more exothermic ring-opening route to the vinoxy radical.[25] The distinctly lower rotational energy of the HCl cannot, in this case, be accounted for by a low-magnitude dipole moment of the oxiranyl radical (c-C_2H_3O), which is computed to be 1.72 D, and to lie close to the plane of the ring, nearly bisecting the ∠C−O−C angle. A definitive explanation of the experimental observations awaits further experimental and theoretical data but is tentatively attributed to the different rotational dynamics of the cyclic and linear radicals. Computed TS structures for the reactions of Cl atoms with oxirane and oxetane are plotted in Figure 10. The Cl−H−C moiety in the transition state is calculated to lie almost perpendicular to the plane of the three-membered ring, and as the C−H bond ruptures, any resultant force will be at the apex of the triangle, inducing a rotational motion of the radical about a line through the triangular structure that does not immediately reorient the negative end of the dipole (the O-atom apex) toward the departing HCl.[41] This behavior is observed in trajectory

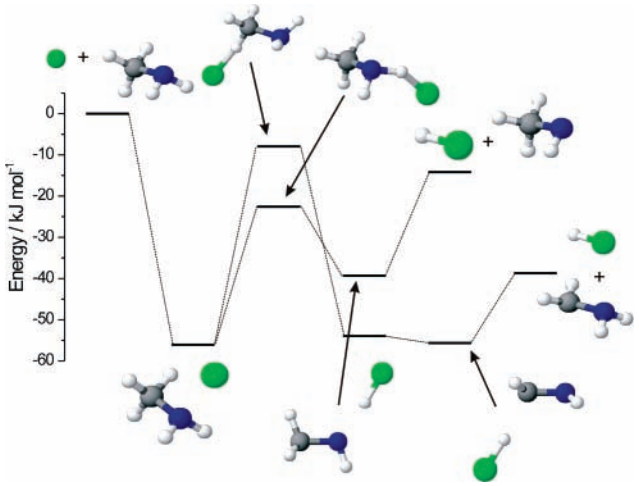

Figure 7. Computed energies and structures corresponding to stationary points on the PES for reaction of Cl atoms with methylamine. The calculations were performed at the G2//MP2/6-311G(d,p) level of ab initio electronic structure theory. Two pathways are illustrated, leading to formation of HCl and either the methanaminyl or aminomethyl radical.

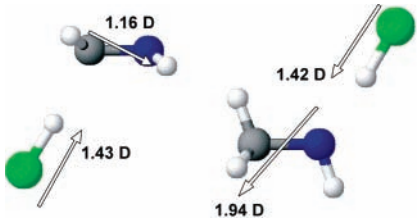

Figure 8. Computed MP2/6-311G(d,p) dipole moments for the radicals and HCl molecules that make up the weakly bound post-TS molecular complexes for the two reaction paths shown in Figure 7 of Cl with methylamine.

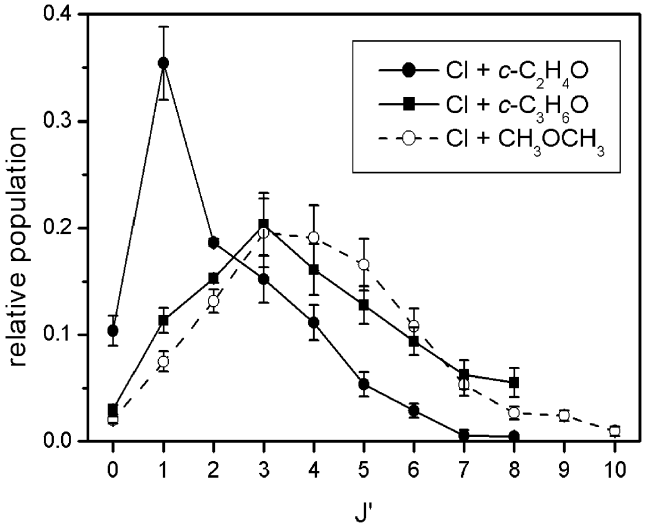

Figure 9. Distributions of relative populations of the rotational levels of the HCl($v' = 0$) products of reactions of Cl atoms with cyclic compounds (●) oxirane and (■) oxetane and, for purposes of comparison, with (○) dimethyl ether. J' denotes the HCl rotational quantum number. The distributions are normalized as in Figure 4.

calculations initiated at the transition state, as described previously. As a result, the HCl does not feel the most anisotropic part of the post-TS potential and thus experiences a lower rotational acceleration than for the methanol and dimethyl ether reactions.

In contrast, reactions of Cl atoms with oxetane produce HCl molecules with rotational energies almost indistinguishable from

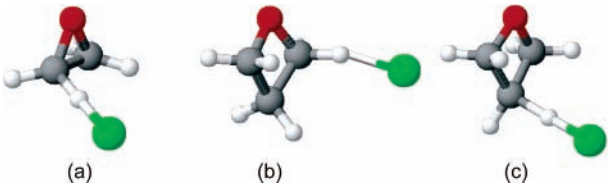

Figure 10. Structures of the transition states for reaction of Cl atoms with (a) oxirane; (b) α-abstraction from oxetane; (c) β-abstraction from oxetane. Structures are computed by MP2/6-311G(d,p) ab initio electronic structure theory methods.

the products of the reaction with DME. There are two competing reaction pathways, corresponding to H-atom abstraction from either the C-atom in the α or the β-position relative to the O atom, giving, respectively, the oxetan-1-yl or oxetan-2-yl radical. For straight chain alcohols and ethers, abstraction at the α-position is expected to dominate the reactivity, but the branching for the abstraction from oxetane is not known. As is confirmed by trajectories, abstraction from the α-position causes the oxetan-1-yl to rotate most naturally about an axis along the diagonal of the four-membered ring that joins the O atom and the β-C atom and does not reorient the negative end of the radical dipole moment toward the HCl. Abstraction from the β-C atom, however, causes oxetan-2-yl rotation about the C−C diagonal and does bring the O-atom into close proximity with the HCl. Computed rotational distributions for the β-abstraction channel are thus much hotter, despite the exothermicity being lower than for the α-abstraction channel. A definitive experimental separation of the two pathways, however, will require selective deuteration of the α- or β-C sites and discrimination between HCl and DCl reaction products using REMPI and TOF mass spectrometric detection.

3.4. Center-of-Mass Frame Scattering. The imaging apparatus described in section 2 allows measurement of the angular scattering of the HCl products in the CM frame, and from the distribution of speeds (contained within the radial dependence of the image), the kinetic energy release into the products can be derived. A representative image and angular and KE distributions are shown in Figure 11. For reaction of Cl atoms with CH_3OH, the scattering is forward and backward peaked in the CM frame, but with significant sideways scattering as well.[22] The distribution in the backward hemisphere agrees very well with the measurements of Suits and co-workers,[42] whose experiments were not able to separate forward scattered reactive signal from strongly interfering, nonreactive signals. The reactions of Cl atoms with CH_3Cl and CH_3Br also show broad angular scatter, but with preferential flux in the backward direction. The broad distributions in both cases are interpreted in terms of a range of impact parameters leading to reaction (as illustrated in Figure 2), but the small barriers to reaction for the Cl + CH_3Cl and CH_3Br reactions are more effectively surmounted by smaller impact parameter collisions, leading preferentially to rebound dynamics. Measurements for HCl formed quantum state specifically in $v' = 0$, $J' = 2-5$ show little variation in the angular scattering, an observation that is contrary to what is seen for the reaction of Cl atoms with ethane, for which the preferential scattering switches from forward to backward as J' increases from $J' = 2$ to 6.[43] The more repulsive interactions associated with small impact parameter (head-on) collisions have been argued to result in greater HCl rotation, but this effect may be washed out for the functionalized molecules by the long-range, post-TS anisotropic interactions associated with the polar fragments that change the rotational energies of the departing HCl molecules late on in the collisional process.

The total kinetic energy releases are broad but peak at quite low values. On average, the fraction of the total available energy channelled into translational energy of the products (averaged over all scattering angles) is $f_t = 0.37$ for the Cl + CH_3OH reaction and $f_t = 0.25$ for Cl + CH_3Cl. The internal energy of the HCl is known from the measurement, because this product is detected with quantum-state specificity, and the balance of the energy (respective fractions of 0.49 and 0.69) is thus internal motion of the radical coproduct. Whether this energy is contained within the numerous vibrational modes or in rotational motion is not established from the experiments, but the trajectory calculations suggest that a large part is in rotation of the radical. The efficient coupling of the available energy into rotation is a consequence of the force applied by the departing H atom along a line well displaced from the center of mass of the radical. There may also be excitation of the wagging motions of the CH_2 group, as posited for the reaction of F atoms with ethane and supported by a Franck−Condon dynamical model.[29]

3.5. Nonadiabatic Reaction Dynamics. An outstanding question for reactions such as those described in preceding sections is whether the dynamics occur purely on the ground PES or whether nonadiabatic dynamics can result in participation of one or more low-lying PESs corresponding to electronically excited states. The reactions of halogen atoms provide a convenient way to explore such effects: in the reaction with CH_4, the ground-state potential correlates with X($^2P_{3/2}$) atoms, whereas spin−orbit excited atoms, X*($^2P_{1/2}$), must react on excited PESs. There have thus been several attempts to characterize the reactivity of F* and Cl* atoms, with mixed success. There is now, however, clear evidence from both kinetic measurements[44] and dynamical studies[7,45] of the reactivity of Cl* atoms, and thus of contributions from nonadiabatic pathways. These effects have recently been reported for the methane

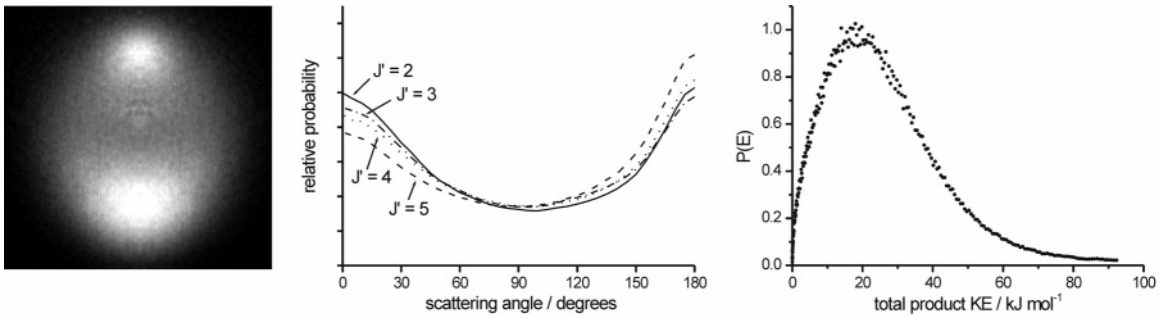

Figure 11. Left: velocity map image for the HCl($v' = 0$, $J' = 2$) products of reaction of Cl atoms with methanol. The relative velocity vector lies along the central vertical axis and the middle of the image corresponds to the center of mass. Analysis of this and similar images provides the CM frame angular scattering probabilities illustrated in the middle panel for HCl($v' = 0$, $J' = 2-5$), and the kinetic energy distribution of the CH_2OH + HCl($v' = 0$, $J' = 3$) products shown on the right.

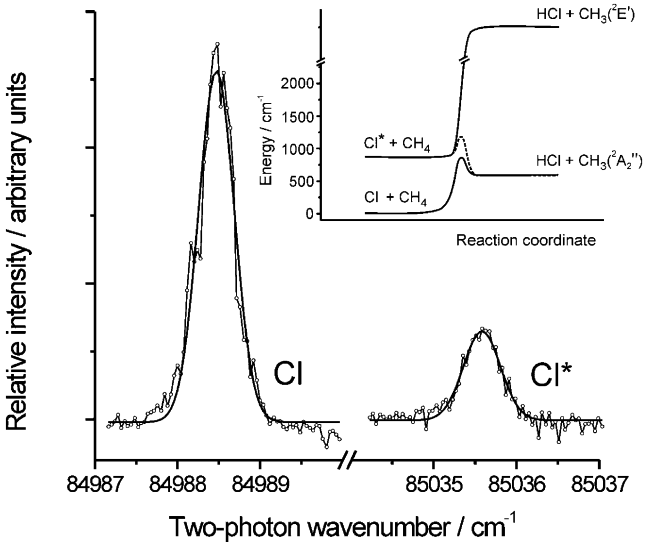

Figure 12. Main figure: 2+1 REMPI signals for $Cl(^2P_{3/2})$ and $Cl^*(^2P_{1/2})$ atomic products of the reaction of CH_3 with HCl. The raw experimental data are plotted as connected open points, and the smooth curves are Gaussian fits used to integrate the peak intensities to obtain a branching ratio. Inset: adiabatic correlation diagram for reactions of Cl and Cl* with CH_4. The dashed line indicates a schematic nonadiabatic pathway for successful reaction of Cl* atoms.

reaction $Cl + CH_4 \rightarrow HCl + CH_3$, with studies conducted on both the forward[45] and the reverse[7] reactions. In this example, experiments conducted at collision energies just above the barrier showed no evidence of Cl* reaction,[46,47] despite its greater internal energy, but if sufficient collision energy is provided to the reagents, nonadiabatic effects can become significant. As yet, it is not clear whether the nonadiabatic interactions occur at long range (as is now known to be common for photodissociation of molecules such as HCl and Cl_2)[48] or in the region of the transition state where the electronic wave function for the system changes character rapidly with nuclear configuration.[49] The inset to Figure 12 illustrates the correlations for reaction of Cl/Cl* with CH_4, and the main figure shows the formation of both Cl and Cl* products for the reverse reaction of CH_3 with HCl. The yield of Cl*, expressed as a fraction of the total chlorine atom yield, was measured using calibrated REMPI transitions to be 0.15 ± 0.02 at collision energies in excess of 78 kJ mol^{-1}. Current experiments are exploring the scattering dynamics of (or leading to) Cl and Cl*, seeking differences that might reveal subtle details of the nonadiabatic mechanisms.

4. Conclusions and Future Directions

A series of systematic measurements of the rotational excitation of HCl molecules formed from the reactions of Cl atoms with various small, heteroatom-functionalized organic molecules (alcohols, amines, alkyl halides) reveals a correlation with the dipole moments of the polar radical product. The reactions of interest involve H-atom abstraction from a carbon atom and pass through transition states that are close to collinear in the Cl−H−C moiety. It is therefore argued that the rotational energy of the HCl, which is considerably greater than is observed for benchmark reactions of Cl atoms with alkanes despite passing through similar transition-state structures, is a consequence of anisotropic electrostatic interactions between the separating reaction products. Reorientation dynamics occur in a time scale comparable to the separation of the products, and trajectory calculations suggest the importance of rotational reorientation of the heteroatom-containing radical in inducing subsequent HCl rotation. In essence, the heteroatom is brought into proximity with the positive end of the HCl dipole, resulting in an interaction that resembles hydrogen bonding, and which transmits a torque to the HCl. Experimental and preliminary computational results for the reactions of Cl atoms with the constrained cyclic ethers oxirane and oxetane suggest that the different reorientation dynamics of the two-dimensional, rigid frameworks of these molecules have consequences for post-transition-state interactions with the HCl.

The spatial orientations of the dipole moments of separating reaction products, not just their magnitudes, must be considered to explain the degrees of rotational excitation of the HCl products from the reactions described herein, or to predict outcomes for unstudied reactions, as is illustrated for Cl atom abstraction of an H atom from methylamine. The results obtained from an extensive body of work thus shed much light on the importance of molecular structure and polarity in controlling the stereodynamics of direct abstraction reactions. The dynamics will not be well represented by approximate calculations in which the polyatomic molecule is treated as a pseudo-diatomic molecule. Ongoing developments in the spectroscopy of weakly bound complexes of the type proposed to influence the reaction dynamics should permit the species associated with shallow pre- and post-TS wells on the PES to be isolated and better characterized.

There are several key advances anticipated in studies of chemical reaction dynamics that will greatly extend the work summarized here. The preceding section touched on progress in the investigation of nonadiabatic dynamics, and thus the role played by excited electronic PESs in nominally "elementary" reactions. The ability to distinguish the scattering dynamics associated with adiabatic and nonadiabatic pathways will be highly instructive, as will angular momentum polarization measurements, which have proven a powerful method of exploring nonadiabaticity in photodissociation.[50] The complexity of polyatomic organic molecules opens up the possibility of multiple, competing pathways for reaction, as observed for $Cl + CH_3NH_2 \rightarrow HCl + CH_3NH/CH_2NH_2$. In other reactions, certain channels remain stubbornly closed, as exemplified by the formation of hydroxymethyl, but not methoxy, radicals from reaction of Cl atoms with methanol. The groundwork now established for these systems prepares the way for either coherent or vibrational mode control experiments to promote one or another reaction path, or to open up apparently closed channels, using laser fields to manipulate the properties of the reagents and transition states.

A further exciting prospect is the transfer of understanding gained from studies of isolated collisions in the gas phase to the more complex environment of the liquid phase. Many of the organic molecules so far studied can be readily condensed, and new observational techniques using ultrafast laser pulses, already demonstrated to work for solution phase studies of the reaction of Cl atoms with dichloromethane, other alkanes, chlorinated alkanes, and alcohols,[51] suggest the future capability of measuring stereodynamical information in solution.

Acknowledgment. We are very grateful to Dr. Jeremy N. Harvey and Keith N. Rosser for major contributions to the work described in this article. Velocity map imaging results were obtained in collaboration with Prof. Theofanis N. Kitsopoulos, Dr. Rachel L. Toomes and Dr. Alrik J. van den Brom at the Ultraviolet Laser Facility, FORTH, Crete. We thank Bristol colleagues Prof. Michael N. R. Ashfold and Dr. Colin M. Western for many valuable discussions. Financial support was

provided by the EPSRC Portfolio Partnership grant *LASER*, and the European Union Marie Curie Research and Training Network *PICNIC*.

References and Notes

(1) Levine, R. D. *J. Phys. Chem.* **1990**, *94*, 8872.
(2) Orr-Ewing, A. J. *J. Chem. Soc., Faraday Trans.* **1996**, *92*, 881.
(3) Althorpe, S. C.; Clary, D. C. *Annu. Rev. Phys. Chem.* **2003**, *54*, 493.
(4) Fernández-Alonso, F.; Zare, R. N. *Annu. Rev. Phys. Chem*. **2002**, *53*, 67.
(5) Liu, K.; Skodje, R. T.; Manolopoulos, D. E. *PhysChemComm* **2002**, *5*, 27.
(6) Alexander, M. H.; Capecchi, G.; Werner, H.-J. *Science* **2002**, *296*, 715.
(7) Retail, B.; Pearce, J. K.; Murray, C.; Orr-Ewing, A. J. *J. Chem. Phys*. **2005**, *122*, 101101.
(8) Juanes-Marcos, J. C.; Althorpe, S. C. *J. Chem. Phys*. **2005**, *122*, 204324.
(9) Ausfelder, F.; Pomerantz, A. E.; Zare, R. N.; Althorpe, S. C.; Aoiz, F. J.; Banares, L.; Castillo, J. F. *J. Chem. Phys.* **2004**, *120*, 3255 and references therein.
(10) Alexander, M. H.; Manolopoulos, D. E.; Werner, H.-J. *J. Chem. Phys.* **2000**, *113*, 11084 and references therein.
(11) Aldegunde, J.; de Miranda, M. P.; Haigh, J. M.; Kendrick, B. K.; Sáez-Rábanos, V.; Aoiz, F. J. *J. Phys. Chem. A* **2005**, *109*, 6200.
(12) Strazisar, B. R.; Lin, C.; Davis, H. F. *Science* **2000**, *290*, 958.
(13) Zhang, D. H.; Collins, M. A.; Lee, S.-Y. *Science* **2000**, *290*, 961.
(14) Camden, J. P.; Bechtel, H. A.; Zare, R. N. *Angew. Chem.* **2003**, *42*, 5227.
(15) Shiu, W.; Lin, J. J.; Liu, K. P.; Wu, M.; Parker, D. H. *J. Chem. Phys*. **2004**, *120*, 117.
(16) Zhou, J.; Zhang, B.; Lin, J. J.; Liu, K. *Mol. Phys.* **2005**, *103*, 1757.
(17) Murray, C.; Orr-Ewing, A. J. *Int. Rev. Phys. Chem*. **2004**, *23*, 435.
(18) Rudić, S.; Ascenzi, D.; Orr-Ewing, A. J. *Chem. Phys. Lett*. **2000**, *332*, 487.
(19) Rudić, S.; Murray, C.; Ascenzi, D.; Anderson, H.; Harvey, J. N.; Orr-Ewing, A. J. *J. Chem. Phys*. **2002**, *117*, 5692.
(20) Rudić, S.; Murray, C.; Harvey, J. N.; Orr-Ewing, A. J. *Phys. Chem. Chem. Phys*. **2003**, *5*, 1205.
(21) Rudić, S.; Murray, C.; Harvey, J. N.; Orr-Ewing, A. J. *J. Chem. Phys*. **2004**, *120*, 186.
(22) Murray, C.; Orr-Ewing, A. J.; Toomes, R. L.; Kitsopoulos, T. N. *J. Chem. Phys*. **2004**, *120*, 2230.
(23) Murray, C.; Retail, B.; Orr-Ewing, A. J. *Chem. Phys*. **2004**, *301*, 239.
(24) Toomes, R. L.; van den Brom, A. J.; Kitsopoulos, T. N.; Murray, C.; Orr-Ewing, A. J. *J. Phys. Chem. A* **2004**, *108*, 7909.
(25) Pearce, J. K.; Murray, C.; Stevens, P. N.; Orr-Ewing, A. J. *Mol. Phys.* **2005**, *103*, 1785.
(26) Marshall, M. D.; Davey, J. B.; Greenslade, M. E.; Lester, M. I. *J. Chem. Phys.* **2004**, *121*, 5845.
(27) Merritt, J. M.; Kupper, J.; Miller, R. E. *Phys. Chem. Chem. Phys*. **2005**, *7*, 67.
(28) Levine, R. D. *Molecular Reaction Dynamics*; Cambridge University Press: Cambridge, 2005.
(29) Whitney, E. S.; Zolot, A. M.; McCoy, A. B.; Francisco, J. S.; Nesbitt, D. J. *J. Chem. Phys*. **2005**, *122*, 124310.
(30) Atkinson, R.; Baulch, D. L.; Cox, R. A.; Hamspon, R. F., Jr.; Kerr, J. A.; Rossi, M. J.; Troe, J. *J. Phys. Chem. Ref. Data* **2000**, *29*, 167.
(31) Orr-Ewing A. J.; Zare, R. N. *Annu. Rev. Phys. Chem.* **1994**, *45*, 315.
(32) *J. Phys. Chem.* **1987**, *91*, 5365−5515.
(33) *J. Chem. Soc., Faraday Trans.* **1989**, *85*, 925−1376.
(34) *Faraday Discuss., Chem. Soc*. **1999**, *113*, 1−498.
(35) Jordan, M. J. T.; Thompson, K. C.; Collins, M. A. *J. Chem. Phys*. **1995**, *102*, 5647.
(36) Thompson, K. C.; Jordan, M. J. T.; Collins, M. A. *J. Chem. Phys*. **1998**, *108*, 8302.
(37) Kerkeni, B.; Clary, D. C. *Mol. Phys*. **2005**, *103*, 1745.
(38) Varley, D. F.; Dagdigian, P. J. *J. Phys. Chem.* **1995**, *99*, 9843.
(39) Picconatto, C. A.; Srivastava, A.; Valentini, J. J. *J. Chem. Phys.* **2001**, *114*, 1663.
(40) Rakitzis, T. P.; Kandel, S. A.; Lev-On, T.; Zare, R. N. *J. Chem. Phys.* **1997**, *107*, 9392.
(41) Pearce, J. K.; Murray, C.; Orr-Ewing, A. J. *Physica Scripta*, in press.
(42) Ahmed, M.; Peterka, D. S.; Suits, A. G. *Phys. Chem. Chem. Phys*. **2000**, *2*, 861.
(43) Bass, M. J.; Brouard, M.; Vallance, C.; Kitsopoulos, T. N.; Samartzis, P. C.; Toomes, R. L. *J. Chem. Phys.* **2003**, *119*, 7168.
(44) Taketani, F.; Takahashi, K.; Matsumi, Y.; Wallington, T. J. *J. Phys. Chem. A* **2005**, *109*, 3935.
(45) Zhang, B. L.; Liu, K. P. *J. Chem. Phys*. **2005**, *122*, 101102.
(46) Kim, Z. H.; Alexander, A. J.; Bechtel, H. A.; Zare, R. N. *J. Chem. Phys.* **2001**, *115*, 179.
(47) Zhou, J.; Lin, J. J.; Zhang, B.; Liu, K. *J. Phys. Chem. A* **2004**, *108*, 7832.
(48) Regan, P. M.; Ascenzi, D.; Brown, A.; Balint-Kurti, G. G.; Orr-Ewing, A. J.; *J. Chem. Phys.* **2000**, *112*, 10259.
(49) Butler, L. J. *Annu. Rev. Phys. Chem.* **1998**, *49*, 125.
(50) Wouters, E. R.; Ahmed, M.; Peterka, D. S.; Bracker, A. S.; Suits, A. G.; Vasyutinskii, O. S. In *Imaging in Chemical Dynamics*; Suits, A. G., Continetti, R. E., Eds.; ACS Symposium Series: American Chemical Society: Washington, DC, 2001; No. 770, p 238 and references therein.
(51) Sheps, L.; Crowther, A. C.; Elles, C. G.; Crim, F. F. *J. Phys. Chem. A* **2005**, *109*, 4296.